



# The influence of wintertime SST variability in the Western North Pacific on ENSO diversity

Boniface Fosu<sup>1</sup> · Jie He<sup>1</sup> · S.-Y. Simon Wang<sup>2</sup>

Received: 2 August 2019 / Accepted: 24 February 2020 / Published online: 2 March 2020  
© The Author(s) 2020

## Abstract

Sea surface temperature anomalies (SSTa) in the Western North Pacific (WNP) have been linked to the development of El Niño Southern Oscillation (ENSO) events a full year in advance. However, the contribution of the WNP precursor to the temporal evolution and spatial complexity of ENSO remains unclear. Using the preindustrial experiment of the Community Earth System Model as the control climate, a partially coupled experiment is conducted in which WNP SSTa are restored to the model climatology. By comparing the perturbed experiment to the control, we are able to clearly characterize ENSO's response to WNP SST variability. We find that the WNP is predominantly linked to eastern Pacific (EP) ENSO events. Without SST variability in the WNP, central Pacific (CP) ENSO events are more likely to develop. This variation in ENSO flavor is controlled by how the WNP projects onto wind stress anomalies in the western equatorial Pacific, which in turn impacts the discharge and recharge of ocean heat during the ENSO cycle. Specifically, the removal of SSTa in the WNP weakens the buildup of ocean heat in the western equatorial Pacific, which then hinders the development of EP-type events.

## 1 Introduction

Several studies have linked the onset of El Niño Southern Oscillation (ENSO) events to extratropical atmospheric and oceanic variability. Specifically, stochastic forcing from the second leading mode of atmospheric variability over the North Pacific, the North Pacific Oscillation (NPO) (Rogers 1981) is thought to significantly influence the state of the tropical Pacific several months prior to the maturation of ENSO; this happens via the so-called Seasonal Footprinting Mechanism (SFM). The SFM describes an SST anomaly “footprint” in spring that is created by atmospheric fluctuations of the NPO in winter and persists through summer, sustaining sea level pressure (SLP) and wind stress anomalies

that are conducive to the initiation of ENSO events (Anderson 2003; Vimont et al. 2003; Alexander et al. 2010).

Closely dovetailed with the SFM is the Pacific Meridional Mode (PMM) (Chiang and Vimont 2004; Chang et al. 2007; Di Lorenzo et al. 2015). The PMM involves NPO-induced modulation of the trade winds that lead to the establishment of SST anomalies (SSTa) in the east central subtropical North Pacific. These anomalies then propagate southward via a wind-evaporation-SST feedback (WES) mechanism (Xie and Philander 1994) and promote the initiation of ENSO events as they reach the equator. An analogous meridional mode can be found in the South Pacific with a similar mechanism to the PMM, i.e. the South Pacific Meridional Mode (SPMM) (Zhang et al. 2014; You and Furtado 2017).

In addition, wintertime SST variability in the subtropical northwestern Pacific, i.e. the Western North Pacific (WNP) mode has been linked to the development of ENSO events the following winter (Wang et al. 2012). The WNP is manifest as a northwest-southeast SST dipole located off southeastern Asia, with an association to equatorial winds believed to strongly influence oceanic Kelvin wave activity that precedes ENSO events (Pegion and Selman 2017; McPhaden 2004; Alexander et al. 2010).

Studies that first related ENSO to subtropical triggers did not consider the occurrence of two different ENSO modes in the tropical coupled ocean–atmosphere system. Apart from

---

**Electronic supplementary material** The online version of this article (<https://doi.org/10.1007/s00382-020-05193-7>) contains supplementary material, which is available to authorized users.

---

✉ Boniface Fosu  
[boniface.fosu@eas.gatech.edu](mailto:boniface.fosu@eas.gatech.edu)

<sup>1</sup> School of Earth and Atmospheric Sciences, Georgia Institute of Technology, Atlanta, GA, USA

<sup>2</sup> Department of Plants, Soils, and Climate and Utah Climate Center, Utah State University, Logan, UT, USA

the generic canonical El Niño events, which are characterized by warmest SSTa in the Eastern Pacific (EP), there also exist central Pacific (CP) El Niño events, which have their largest SSTa near the Dateline (Larkin and Harrison 2005; Ashok et al. 2007; Kao and Yu 2009; Kug et al. 2009; Kar-nauskas 2013).

For a better understanding of the spatio-temporal complexity of ENSO, several researchers have called for a closer look into the linkages between the precursor dynamics of ENSO and ENSO diversity (Timmermann et al. 2018). For example, are there specific precursors or triggers for EP and CP events, or are these differences happening by chance, and how would the existence of these precursors impact our ability to predict these different events (Kirtman 2019)? While the PMM has emerged as a key driver in the generation of the CP type ENSO (Yu and Kim 2011; Kim et al. 2012; Vimont et al. 2014; Stuecker 2018), the SPMM has been linked to amplified SSTa in the eastern Pacific (Zhang et al. 2014). However, unlike these meridional modes, the mechanisms by which the more distantly located WNP SSTa influences the various types of ENSO are still poorly understood. Apart from augmenting our understanding of the range of ENSO variations, extratropical and subtropical precursors to ENSO can directly be utilized to improve long-lead ENSO predictions.

Against this backdrop, this study is designed to determine the contribution of SST variability in the WNP to the temporal evolution and spatial diversity of ENSO using the fully coupled global climate Community Earth System Model (CESM) (Gent et al. 2011). The outline of this manuscript is as follows. In Sect. 2, we present a brief description of the utilized observational datasets, model experiments and key analytical methods. In Sect. 3, we present and discuss the results of our experiments. We summarize the results in Sect. 4 and present conclusions.

## 2 Data and methodology

### 2.1 Observational datasets

The Hadley Centre Sea Ice and Sea Surface Temperature dataset (HadISST) is used to describe variations in global SST (Rayner et al. 2003). HadISST consists of monthly mean values from 1870 to present. For analysis of ocean warm water volume (WWV) and subsurface temperature, we utilize the NCEP Global Ocean Data Assimilation System at the resolution of  $0.333^\circ$  latitude  $\times$   $1.0^\circ$  longitude with vertical levels ranging from 5 to about 4500 m depth, available from 1980 to present (Behringer and Xue 2004). Sea level pressure and 10-m wind components are taken from the National Center for Environmental Prediction-National Center for Atmospheric Research (NCEP-NCAR) reanalysis

product (Kalnay et al. 1996) and consist of monthly mean values from 1948 to present on a  $2.5^\circ \times 2.5^\circ$  horizontal grid globally.

### 2.2 Partially coupled experiment

To estimate ENSO's response to SST variability in the WNP, we perform a partially coupled perturbation experiment with the Community Earth System Model (CESM version 1.2.2) using pre-industrial radiative forcing. In the CESM, the atmospheric model component is configured with CAM4 physics on a  $1.9^\circ \times 2.5^\circ$  horizontal grid and 26 levels in the vertical; coupled to dynamic ocean (POP2) and sea ice (CICE) models on a nominal horizontal resolution of  $1^\circ$  and 60 vertical levels. Wang et al. (2013) used the CESM to investigate the WNP influence on ENSO development in the historical single-forcing experiments.

The first experiment, the control, is run for 272 years. The second, the “noWNP” experiment, branches from the control at year 52 and is integrated for 220 years. The noWNP experiment is set up by restoring SST in the WNP region to the monthly mean climatology of the control using a restoring time scale of 2 days. Figure 1a shows the region where SST is restored; within the inner box, the weighting coefficient ( $\alpha$ ) is equal to 1 and reduces to zero in a  $10^\circ$  linearly tapering buffer, i.e. from the edge of the inner box to the edge of the outer boxes. In other words, the weighting coefficient ( $\alpha$ ) ranges from 0 to 1, where 1 is full restoration and 0 is no restoration. Outside this region, the model is fully coupled (e.g. Liguori and Di Lorenzo 2019). The last 200 years of both experiments are analyzed.

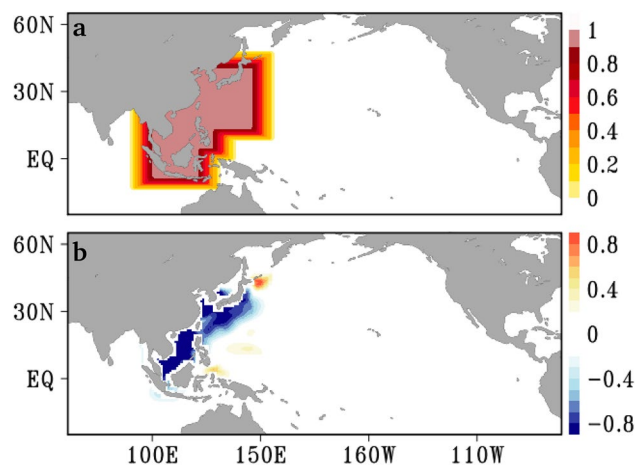


**Fig. 1** **a** The restoring domain and mask used in performing the noWNP experiment. Coefficients of the mask (i.e. weighting coefficients) vary from 1 to 0 when moving from the center to the boundary of the masking region. 1 is full restoration and 0 is no restoration. **b** The mean SST anomalies (°C) for a cold WNP in DJF, i.e. the WNP precursor pattern to El Niño (Wang et al. 2012)

Note that the restoring domain is confined to the region where the WNP mode is considered most active, i.e. the northwestern branch of the WNP (Fig. 1b). This is done for two reasons: first, the eastern subtropical component of the WNP dipole includes the westernmost tip of the ENSO SSTa region, as well as the southeastern lobe of the PMM's SST expression. Secondly, the northwestern branch of the WNP dipole (i.e. along the Kuroshio Current) starts evolving in fall, a few months prior to the establishment of its eastern subtropical counterpart (Ding et al. 2015; Park et al. 2017), making SSTa there the most critical to the evolution of the WNP. Taken together, these steps ensure that SST is reasonably restored within the domain peculiar to the precursor dynamics of the WNP and that no SSTa from the PMM or ENSO is directly imposed.

### 2.3 ENSO and precursor indices

For all variables, anomalies are calculated by removing the long-term monthly climatology over the period being analyzed. Time series of the observed data are then linearly detrended. A commonly used index for representing SST variability associated with ENSO is the 3-month running mean of SSTa in the region, 170° W–120° W to 5° S–5° N, referred to as the “Niño-3.4 index.” An El Niño is said to occur if the Niño-3.4 index, averaged over December–February (DJF) exceeds 1 SD.

To separate ENSO into EP and CP types, we follow the definitions by Takahashi et al. (2011), calculated by first performing EOF analysis on SSTa in the equatorial Pacific, 120° E–70° W, 25° S–25° N. The ENSO indices are then defined as:

$$EP-index = \frac{PC1 + PC2}{\sqrt{2}} \quad (1)$$

$$CP-index = \frac{PC1 - PC2}{\sqrt{2}} \quad (2)$$

where the EP and CP indices correspond to the canonical and central Pacific ENSO, respectively. PC1 (PC2) refers to the principal component time series associated with the first (second) leading pattern of SSTa. Spatial SSTa patterns (i.e. EP pattern and CP pattern) corresponding to the EP and CP indices are obtained by linearly regressing the SST anomaly field onto each index. This approach views El Niño events as the superposition of the two EOF modes, which results in a continuum of ENSO characteristics.

The WNP precursor pattern is defined as the second mode of maximum covariance analysis between low level wind anomalies and SSTa within 90° E–170° W to 10° S–30° N in DJF. The first mode depicts a canonical ENSO structure with a tripole SST pattern in the central tropical Pacific, western

tropical Pacific and South China Sea (Wang et al. 2012). The negative (positive) phase of the WNP is associated with the development of El Niño (La Niña).

The vital role thermocline fluctuations play throughout the ENSO cycle is well established. Here, we use the depth of the 15 °C (Z15) and 20 °C (Z20) isotherms as proxies for thermocline depth; both have extensively been used in the literature for the analysis of thermocline depth variations in the tropical Pacific.

### 2.4 Composite analysis

We analyze the development of ENSO using composites of atmospheric and oceanic variables associated with 30 El Niño events identified in the last 200 years of the noWNP experiment and a corresponding number of 30 events in the control (Fig. S1). The composites are based on the DJF Niño3.4 index and are composed from DJF<sub>yr-1</sub> (i.e. the winter a full year before ENSO reaches its mature phase or peak) to DJF to show the seasonal evolution of ENSO. In between DJF<sub>yr-1</sub> and DJF, composites are also calculated for March–May (MAM), June–August (JJA), and September–November (SON) to complete the evolution cycle. We then compute the difference between the composites of the two experiments at each time step to divulge the WNP influence.

### 2.5 Kelvin waves compositing

The development of Kelvin waves forced by surface winds in the western equatorial Pacific is one of the key mechanisms for ENSO development and growth. We measure the activity of oceanic Kelvin waves by first, Lanczos filtering daily sea surface height (SSH) fields to retain periods between 20 and 120 days, consistent with the frequency of oceanic Kelvin waves activity. The filtered SSH anomalies are then used to construct composites representative of the seasonal variation of Kelvin waves activity in the lead up to El Niño events. We do this by first calculating the variance of all days within each season of the selected El Niño years at each longitude along the equator. The standard deviation is then calculated over the summed variance of the selected events.

## 3 Results

### 3.1 Modeled ENSO response to WNP forcing

Figure 2 compares the El Niño SST composites and the first two EOF modes from the control and the noWNP experiments. The differences in the SST composites of El Niño events in Fig. 2 clearly distinguishes the impact of the WNP mode on ENSO. While the control experiment

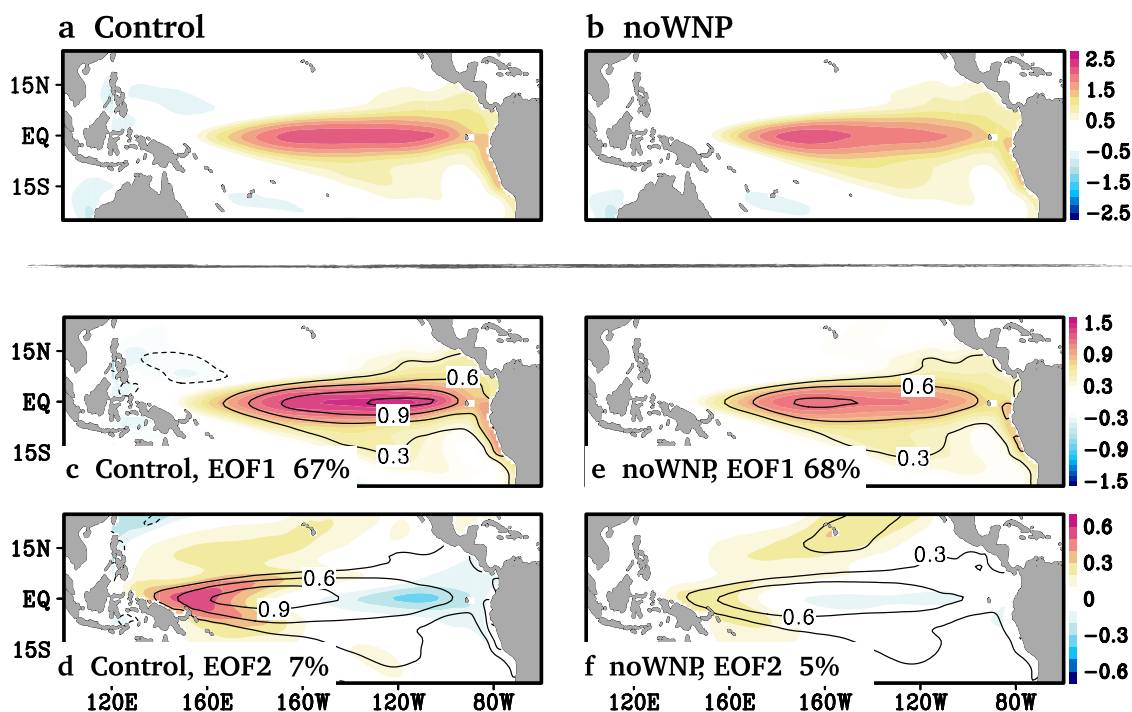


**Fig. 2** a, b SST composites of El Niño events in DJF. An El Niño is said to occur if the DJF Niño-3.4 index exceeds 1 SD. All composites are based on 30 El Niño's in the control and 30 in the noWNP experiment. The first two leading modes of tropical Pacific SSTa in the c, d

control and e, f noWNP experiment. The number in the bottom-left corner of each panel indicates the amount of explained variance. Corresponding EP and CP EOF patterns (as in Takahashi et al. 2011) are superposed in contours. The unit is °C

(Fig. 2a) is characterized by pronounced warming in the eastern Pacific, maximum SSTa in the noWNP experiment are geographically constrained to the central Pacific (Fig. 2b). This suggests that the WNP is predominantly linked to the Eastern Pacific type ENSO. When SST variability in the WNP is muted, CP El Niño's are more likely to develop.

Although the literature is replete with examples of the Niño-3.4 index being used to identify ENSO episodes, it may not be optimal for describing the various ENSO flavors. To better elucidate changes in the pattern of SSTa in the tropical Pacific when SST is suppressed in the WNP, we examine the first two empirical orthogonal functions (EOF) of SSTa in the tropics. We interpret EOF1 in the control experiment as the baseline pattern of ENSO, which combines both the EP and CP El Niño types (shading, Fig. 2c). The second EOF can be added or subtracted from EOF1 to divulge how ENSO events express themselves differently (shading, Fig. 2d). Such variations are achieved with the aforementioned EP and CP patterns (Takahashi et al. 2011).

Both the EP (contours, Fig. 2c) and CP (contours, Fig. 2d) patterns are ENSO-like. While the EP pattern has its strongest amplitude along the eastern equatorial Pacific (east of 150° W), maximum SSTa of the CP pattern are located in the central equatorial Pacific (along 160° E–160° W), mimicking the observed EP and CP ENSO types respectively.

By contrast, EOF1 of the noWNP experiment shows a warming maximum in the central equatorial Pacific that is consistent with the CP type ENSO (shading, Fig. 2e). The zonal east–west equatorial SST dipole that is seen in EOF2 of the control is suppressed without SST variability in the WNP (shading, Fig. 2f). Both the EP (contours, Fig. 2e) and CP (contours, Fig. 2f) patterns favor the spatial expression of CP ENSO due to the apparent suppression of a zonal SST dipole in EOF2, which effectively removes the diversity in ENSO. This is perhaps the clearest indication yet that the WNP is linked to EP El Niño dynamics and an important contributor to ENSO diversity.

### 3.2 Seasonal controls of ENSO to WNP forcing

The evolution of ENSO and its precursor pattern is presented in Fig. 3 through composites of surface temperature anomalies, subsurface potential anomalies and surface winds. By juxtaposing the evolution of ENSO in the control (Fig. 3a) with the noWNP experiment (Fig. 3b), and by examining the differences (Fig. 3c) between the two experiments, one can discern the means by which the absence of SSTa in WNP affects ENSO diversity in the coupled system.

To examine the extent to which the model is fit for the research purpose, we first take a look at the correlation between indices of the WNP and ENSO in the CESM (Fig.

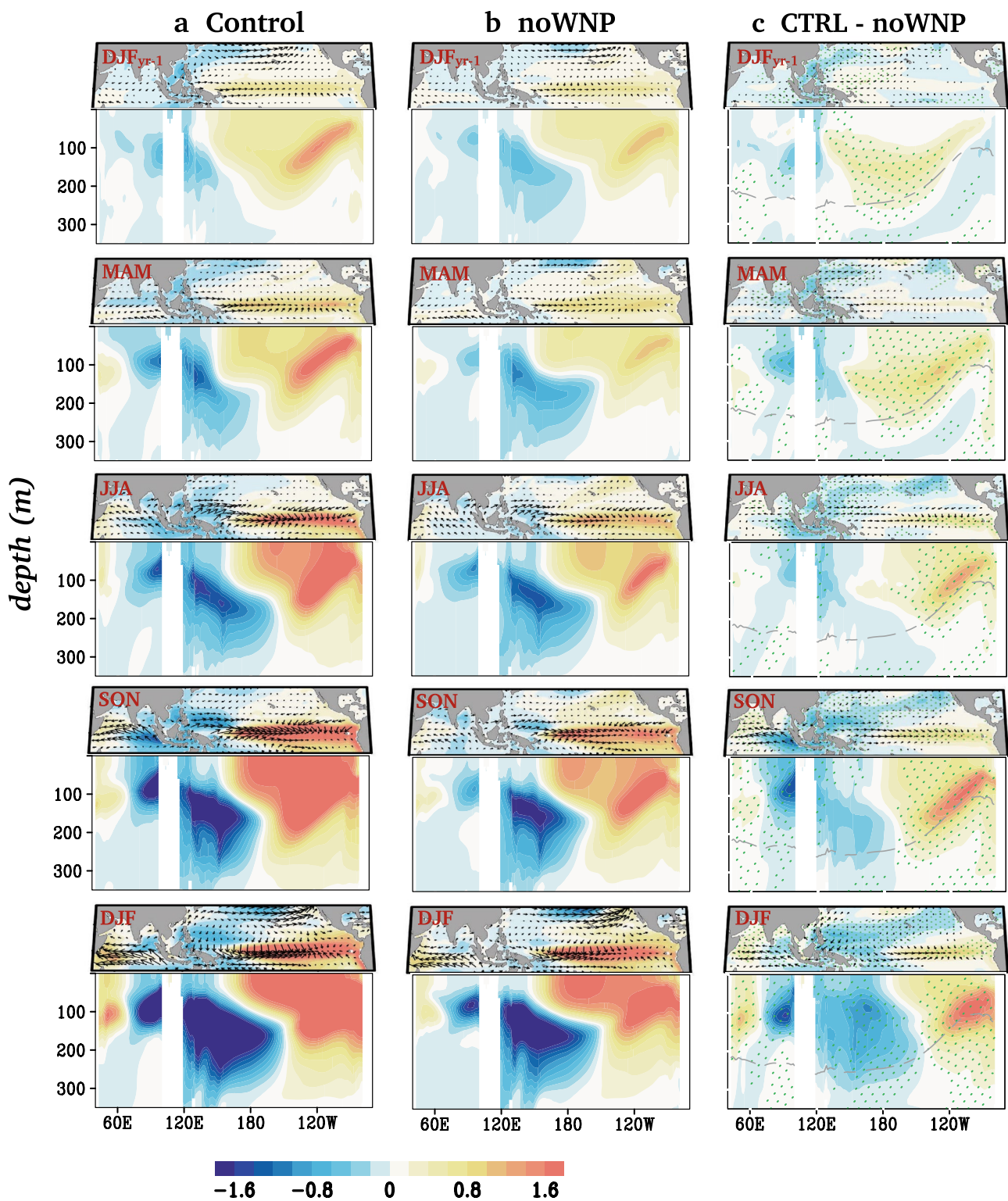


**Fig. 3** Precursor pattern of ENSO in the CESM: El Niño composite of SSTa (top panel—shading, °C), surface winds (vectors, ms<sup>-1</sup>) and the cross section of 2°S–2° N averaged subsurface potential temperature anomalies (bottom panel—shading, °C) in the control and noWNP experiments, and their difference. All composites are based on 30 El Niño’s in the control and 30 in the noWNP experiment. The

mean 20 °C isothermal depth is superimposed on the difference plot. Green stipplings represent statistically significant SST and potential temperature differences at the 95% confidence level based on the Student’s t-test. Likewise only the statistically significant differences in the surface winds are plotted, also at the 95% confidence level

S2) and make a general comparison between the evolution of ENSO in the CESM control and the observed pattern (Fig. S3). The WNP as a precursor has a fairly good correlation with ENSO in the CESM (Fig. S2a). As expected, the optimal correlation between the WNP and ENSO occurs when the WNP lags ENSO by a year (Fig. S2b) as was shown in Wang et al. (2012).

Like in most coupled models, the most conspicuous bias in the CESM is the westward extension and magnitude of SSTa in the tropical equatorial Pacific (Fig. S3b). In observations (Fig. S3a), the core of the warming is over the warm pool in DJF<sub>yr-1</sub> and relatively narrow in the zonal direction as ENSO grows. These biases are primarily linked to an overestimation of the mean zonal wind stress in the model, which in turn generates spurious thermocline anomalies that propagate eastward as downwelling Kelvin waves (Taschetto et al. 2014). Evidence of such rampant Kelvin waves activity can be seen in the early evolution of subsurface temperature anomalies in the control (DJF<sub>yr-1</sub>, Fig. S3b), contrary to the observed pattern (Fig. S3a).

Despite such systematic biases, the CESM's apparent realism in replicating key features of the ENSO cycle and its precursor dynamics (Deser et al. 2012; Wang et al. 2015; Yoon et al. 2015) made it possible to undertake this research; this is encapsulated by the realistic representation of ENSO's phase locking to the seasonal cycle as seen in Fig. S3b. As well, the WNP precursor pattern is realistically simulated (Wang et al. 2013); characteristically featured northeast of Papua New Guinea, with cooling in the northwestern part and warming in the southeastern part during the initial stages of ENSO development (DJF<sub>yr-1</sub>).

Several studies have demonstrated that prior to boreal spring, a charged western tropical Pacific heat content (i.e. Pacific warm pool) is necessary for the subsequent development of El Niño (Vimont et al. 2003; Alexander et al. 2010). In the control experiment (DJF<sub>yr-1</sub>, Fig. 3a), we see a charged western equatorial Pacific characterized by basin-wide subsurface temperature anomalies and a deep thermocline. At the surface, wind vectors are directed from negative SSTa in the vicinity of the WNP toward warmer SSTa at the edge of the warm pool (Fig. 3a). Unlike the control, the noWNP experiment (Fig. 3b) is characterized by a relatively shallow thermocline and a less expansive warm pool, which appears to curtail westerly wind development over the western Pacific (Fig. 3c).

The anomalous northerlies over the WNP begin to wane off after winter (DJF<sub>yr-1</sub>), at the same time the climatological northerlies (not shown) begin to subside. Superimpose the anomalous winds on the climatology, the northerlies will amplify in response to a speed up of evaporation, which then leads to an intensification of the WNP cooling in a manner that is consistent with a positive WES feedback mechanism (Park et al. 2017). So, when the climatological northerlies

begin their seasonal retreat in spring, the anomalous northerlies also die down as the cool SSTa along the east Asian coast gradually begins to reverse sign. This is particularly evident in observations (Fig. S3).

A well-known characteristic of observed ENSO events is the concurrent evolution of the Indian Ocean dipole (IOD) (Yu and Rienecker 1999; Schott et al. 2009; Izumo et al. 2010). Beginning in the summer of an El Niño year, SSTa in the tropical Indian Ocean exhibit an east–west asymmetry, synchronous with easterly wind anomalies over Sumatra and strong westerlies over the western equatorial Pacific. The simulation of this feature in the control (Fig. 3a) is generally in agreement with the observed pattern (Fig. S3), although the easterly wind anomalies off Sumatra are rather weak in observations. Annamalai et al. (2005) argue that the presence of the IOD modulates convective activity over the eastern equatorial Indian Ocean and the tropical western Pacific during the developing phase of El Niño and remotely strengthens westerly anomalies in the western and central Pacific via an atmospheric Kelvin wave. Without SST variability in the WNP, this IOD feature weakens after spring (Fig. 3c), suggesting a WNP-associated process that prolongs the IOD and its effects.

Through air–sea coupling and a positive Bjerknes feedback (Bjerknes 1969), westerly wind anomalies and positive SSTa strengthen and expand eastward, concomitant with the eastward advection of the Pacific warm pool by downwelling Kelvin waves (i.e. the eastward propagation of subsurface oceanic temperature anomalies from DJF<sub>yr-1</sub>) until ENSO reaches its mature phase (DJF). The location of the maximum warming at this stage conforms to the “baseline ENSO” pattern (as in Fig. 2c) in the control (Fig. 3a), and the CP type ENSO (as in Fig. 2d) in the noWNP experiment (Fig. 3b). A comparison between Fig. 3a, b (DJF) yields a manifestation of ENSO diversity, directly introduced into the coupled system by the suppression of SSTa in the WNP (Fig. 3c).

The air–sea coupling during the evolution of ENSO in both experiments are similar, although anomalies from the noWNP experiment are weaker. The initial accumulation of ocean heat, deep and basin-wide in the control but shallow and constrained in the perturbed run, seems to be the initial modulating factor of the subsequent air–sea coupling that eventually leads to diversity in ENSO. This assertion is consistent with Fedorov et al. (2015), who found that initial subsurface ocean conditions could modulate the role of stochastic wind forcing in producing ENSO diversity.

### 3.3 The WNP's impact on ENSO diversity

In this section, an attempt is made to divulge the mechanisms linking WNP SSTa variability to ENSO diversity. In Fig. 4 we use the ENSO based composites of 500-hPa

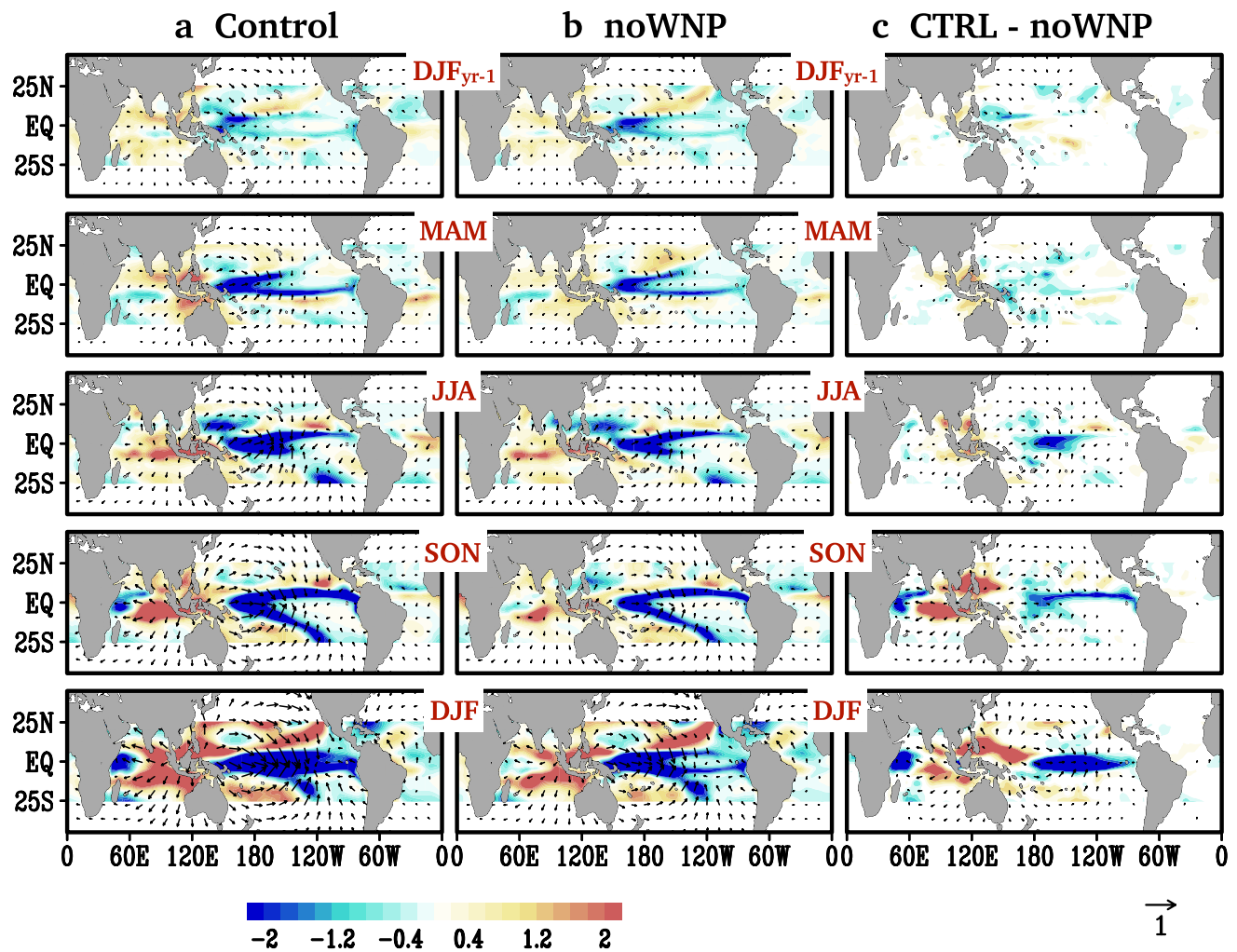


**Fig. 4** El Niño composite of 500-hPa vertical velocity (shading, units:  $10^{-2}$  Pa/s) and 850-hPa divergent winds (vectors, units:  $\text{ms}^{-1}$ ) in the control and noWNP experiments, as well as their difference. All composites are based on 30 El Niño’s in the control and 30 in the

noWNP experiment. Only the statistically significant differences are plotted at the 95% confidence level based on the Student’s t-test. The vector scale is shown at the bottom right side of the figure

vertical velocity and 850-hPa divergent wind anomalies to show the large-scale circulation pattern associated with ENSO evolution. Figure 4 is discussed in tandem with Fig. 5, which is a similar plot but for precipitation and 850-hPa streamfunction. A year before a mature El Niño ( $\text{DJF}_{\text{yr}-1}$ ), when the western equatorial Pacific warm water volume is sufficiently charged (Fig. 3a), anomalous deep atmospheric convection develops over the Pacific warm pool. This induces strong surface divergence and subsidence (Fig. 4a), as well as diabatic cooling (Fig. 5a) over the WNP and the Indian Ocean. The tropical lower-level streamfunction anomalies display a classic Gill Rossby wave response to the heating in the western equatorial Pacific (Gill 1980), i.e. two low-level anticyclonic anomalies straddling the equator west of the convection center and a zone of westerlies lying between them. The

dynamical effect of the westerlies is to flatten the equatorial thermocline by shoaling it in the western equatorial Pacific while deepening it in the east through the generation of equatorial Kelvin waves (Fig. 3a). Consequently, an El Niño can develop as positive subsurface temperature anomalies are upwelled to the surface along the mean thermocline by the eastward propagating Kelvin waves.

The Rossby–Kelvin wave response is symmetric to the tropical heating source as ENSO evolves (Fig. 5a) and amplifies with the eastward expansion of maximum tropical Pacific SSTa (Fig. 3a). This is evident from the eastward migration of the Pacific warm pool and a speedup of the Pacific Walker cell (Fig. 4a). Accompanying the continued growth of positive SSTa are positive precipitation anomalies across the equatorial Pacific and negative anomalies along the poleward flanks of the convergence zones (Fig. 5a).

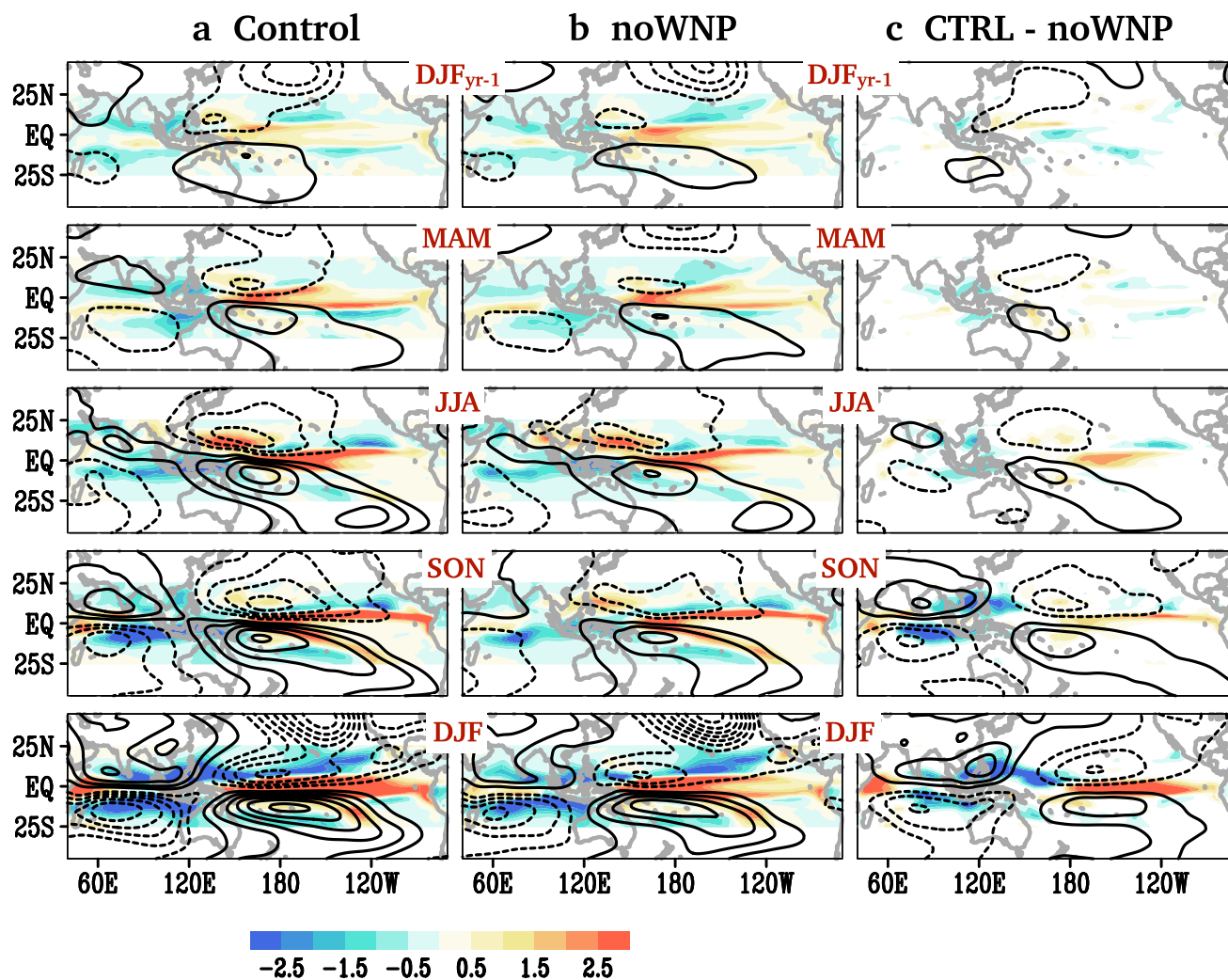


**Fig. 5** Same as Fig. 4 but for precipitation (shading, units:  $\text{mm d}^{-1}$ ) and 850-hPa streamfunction (contours, units:  $10^7 \text{ m}^2 \text{ s}^{-1}$ ). The contour interval is 1. Only the statistically significant differences are plotted at the 95% confidence level based on the Student's *t*-test

The Gill and Walker cell responses in the noWNP experiment track the control throughout ENSO evolution, albeit with a weaker amplitude (Figs. 4c, 5c). This is due to the weak initial convection over the warm pool, arising from a relatively shallow warm water volume in the western equatorial Pacific, and is also why westerlies in the noWNP experiment are weaker during the early stages of El Niño development (Fig. 3c).

Subsurface temperature anomalies constitute a reasonable proxy for tracking the activity of oceanic Kelvin waves as shown in Fig. 3. However, since Kelvin waves are the major means by which ocean heat is transferred from the western Pacific to the central–eastern Pacific, we utilize a more statistically robust metric in measuring oceanic Kelvin waves activity in the lead up to El Niño. That is, the standard deviation of 20–120-day filtered oceanic dynamic height anomalies (Fig. 6). It is inferred from the considerably higher

standard deviation in Fig. 6a that Kelvin waves occur more frequently in the control than in the noWNP run (Fig. 6b). The timing and location of the wave activity are also telling. In the control, strong Kelvin waves activity start early and persist through the year and extend from the central to the eastern Pacific. Strong Kelvin waves are not initiated in the perturbed run until spring, and when they do, are confined to the central equatorial Pacific. Recall that when Kelvin waves carry warm subsurface water from west to east, they are meant to stratify and flatten the thermocline relative to the mean. Weak Kelvin waves are characterized by a zonal tilt of the thermocline that precludes them from achieving such stratification, leading to a greater probability of a CP pattern (Vasquez 2015).

Both realizations of ENSO in the control and perturbed run manifest the Rossby–Kelvin wave response to western equatorial heating, which highlights aspects of the delayed



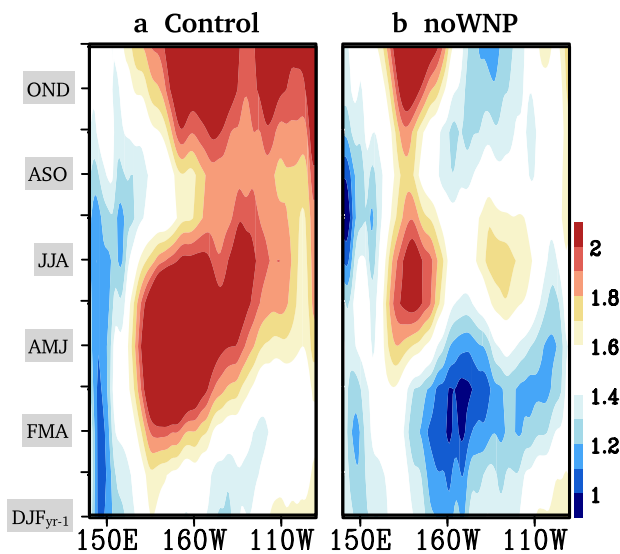


**Fig. 6** Standard deviation of 20–120 days filtered sea surface height anomalies (cm) averaged from 5° S to 5° N, showing Kelvin wave activity in the lead up to El Niño events. DJF<sub>yr-1</sub> is the winter a full year before a mature El Niño

oscillator paradigm of ENSO (Schopf and Suarez 1988; Battisti and Hirst 1989). Likewise, the evolution of subsurface temperature anomalies in both experiments as shown in Fig. 3 is well within the framework of the recharge–discharge theory of Jin (1997). The evolution mechanisms of the two ENSO types are thus comparable. The EP and CP ENSO types are rather separated by differences in the strength of the air–sea coupling by which they evolve (Figs. 3c, 4c, 5c).

It appears the suppression of SSTa in the WNP is effective in damping wind stress anomalies in the western equatorial Pacific, which in turn limits the heat discharge and recharge of the Pacific heat during the ENSO cycle. In a positive feedback loop, the initial buildup of subsurface water modulates the ensuing air–sea interactions; so that, a strong (weak) buildup of ocean heat in the western equatorial Pacific can induce a strong (weak) Gill response and an equally strong (weak) Bjerknes feedback, which are favorable for the development of EP (CP) type events.

### 3.4 Source of thermocline variability

How then does the WNP remotely contribute to the discharge and recharge of the equatorial Pacific? The first two modes of thermocline variability defined through EOF analysis of Z15 anomalies have been interpreted as consistent with the recharge oscillator paradigm of ENSO (Meinen and McPhaden 2000; Capotondi et al. 2006). The first mode in the control (Fig. 7a) is similar to the noWNP experiment (Fig. 7b)—both are characterized by an east–west dipole

representative of changes in the zonal thermocline slope. As a result, this EOF1 mode is often called the “tilting mode,” and represents the mature phase of an El Niño, marked by a deeper thermocline in the central–eastern Pacific and a shallower thermocline in the western Pacific.

On the other hand, EOF2 describes a deepening or shoaling of the equatorial thermocline as a whole (i.e. recharge–discharge mode). The positive phase of EOF2 is characterized by the anomalous zonal slope of the thermocline, which is associated with an anomalous poleward Sverdrup transport that is responsible for discharging warm water from the equatorial thermocline resulting in a shallower-than-average thermocline across the equatorial Pacific. Upwelling of colder water in the eastern Pacific subsequently erodes the original warm SSTa and leads to the opposite phase of the cycle. In this view, the two leading EOFs are expected to be approximately in quadrature (Deser et al. 2012).

The lag correlation analysis between the two principal-component (PC) time series reveals that PC1 leads PC2 by about 10 months in the control (Fig. 7c) and about 12 months in the noWNP experiment (Fig. 7d), with maximum correlations of about 0.8 and 0.6 respectively when PC1 leads. The approximate 10-month lag is in good agreement with the observed ENSO cycle and observations (Meinen and McPhaden 2000). The reduced peak correlations in the perturbed run suggest that in comparison to EP El Niño’s, thermocline feedbacks and the recharge of heat in the equatorial Pacific prior to a CP El Niño are not as intense. This supposition is confirmed by Fig. 8, comprising equatorial Pacific (5° S–5° N) SSTa (shading) and wind stress (vectors) composited based on PC2 (i.e. the recharge–discharge mechanism). The evolution in both the control and noWNP experiments are characterized by relatively simple oscillatory transitions: a positive mode leads to El Niño and is preceded by a La Niña. This is consistent with the existing view that a La Niña event produces a wind stress pattern that tends to charge the equatorial Pacific thermocline (i.e. the positive phase of the recharge–discharge mechanism) and subsequently leads to the onset of an El Niño event, and similarly, to a La Niña from the negative phase (Yu and Fang 2018). We note here that the charging associated with La Niña and the discharging associated with El Niño can be asymmetric in amplitude (Chen et al. 2015; Hu et al. 2017).

The control experiment exhibits a positive SSTa pattern consistent with EP ENSO events, characterized by strong wind stress and negative SSTa anomalies (Fig. 8a), which indicates of a strong recharge of the western equatorial Pacific warm water volume in the lead up to El Niño (Fig. 3a). In a sharp contrast to the control, the noWNP experiment exhibits a central Pacific pattern of maximum SSTa that is preceded by extremely weak wind stress and negative SSTa anomalies (Fig. 8b). The differences between the two experiments are

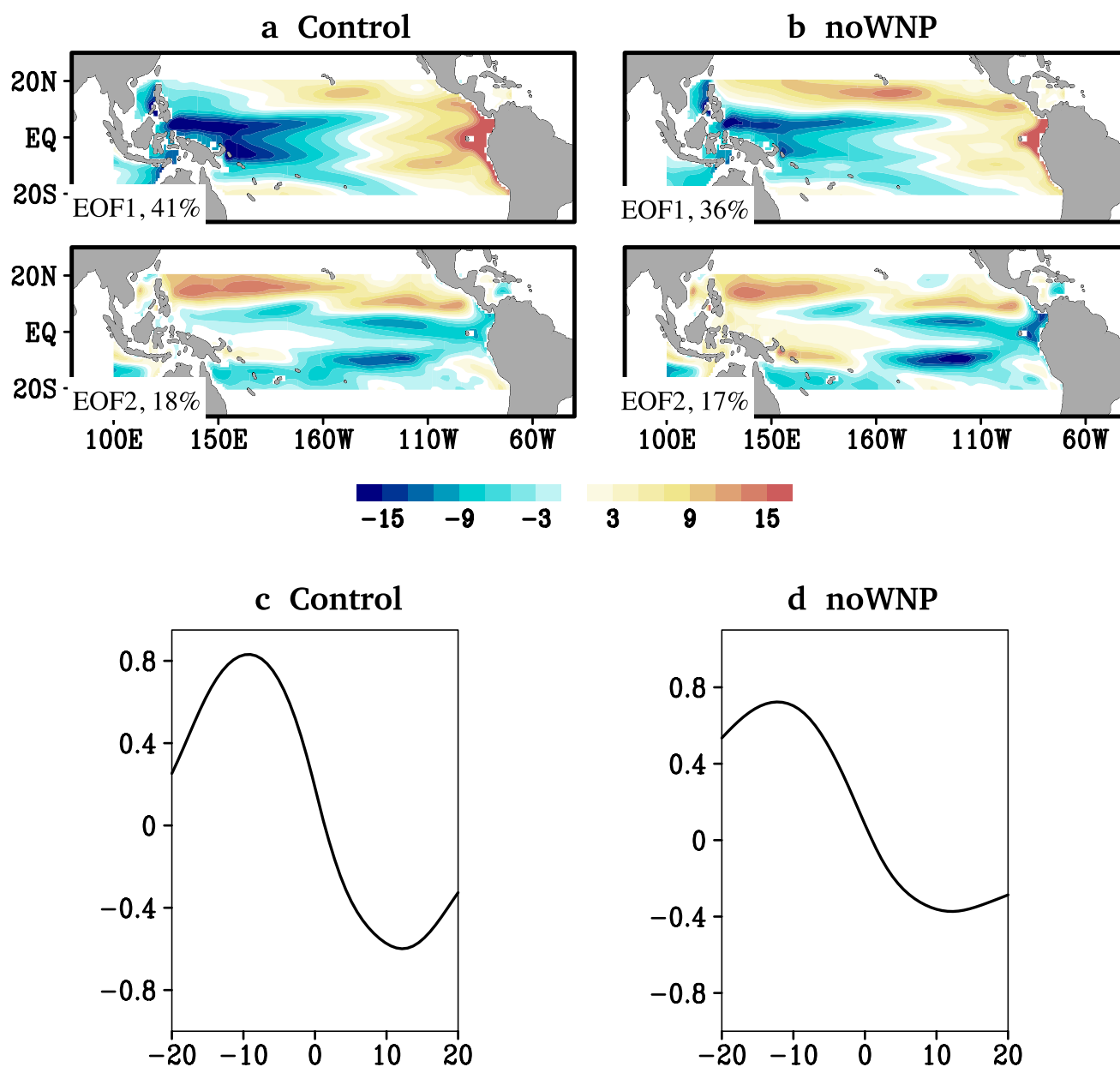


**Fig. 7** **a, b** The two leading EOFs of thermocline depth (Z15 in meters). Blue shading is for negative values (thermocline shallower than average), and indianred shading is for positive values (thermocline deeper than average). The percent variance explained by each

mode is shown on the bottom left corner of each panel. **c, d** Lag-correlation curves between PC1 and PC2; negative (positive) lags are for PC1 leading (lagging) PC2. The lag of maximum correlation, in absolute value, is approximately a quarter of a cycle

readily apparent in Fig. 8c and explains why we notice a relatively weak buildup of ocean heat in the western equatorial Pacific prior to the onset of CP ENSO events (Fig. 3b).

#### 4 Summary and conclusions

The contribution of the WNP precursor mode (Wang et al. 2012, 2013) to the evolution and spatial complexity of ENSO was investigated by running a partially coupled

experiment on NCAR's Community Earth System Model (CESM 1.2.2) under pre-industrial radiative forcing. The CESM was chosen for its apparent realism in simulating the ENSO cycle and its dynamics. The partially coupled experiment, dubbed "noWNP," was set up by restoring SSTa within the bounds of the most active component of the WNP mode to the monthly mean climatology of the control. By comparing the perturbed experiment to the control, we were able to isolate the characteristics of ENSO's response to WNP SST variability with increased confidence.

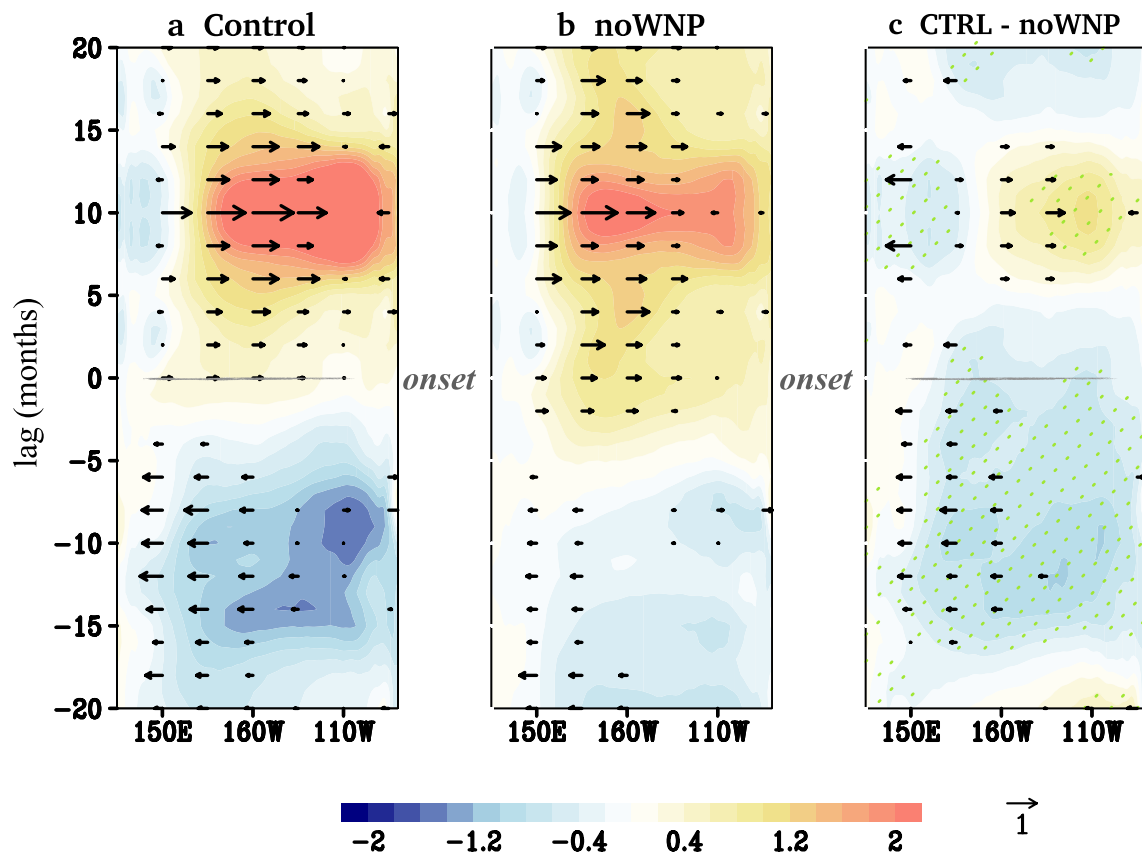


**Fig. 8** The evolution of equatorial Pacific (5° S–5° N) SSTA (shading, °C) and wind stress (vectors, dyne/cm<sup>2</sup>) composited for the positive phase of the rechargedischarge mechanism. Blue (crimson) shading is for La Niña (El Niño) and the recharging phase (discharging phase). The green stippings represent statistically significant SST

differences at the 95% confidence level based on the Student’s t-test. Likewise only the statistically significant differences in the surface winds are plotted, also at the 95% confidence level. The vector scale is shown at the bottom right side of the figure

It was found that the WNP is directly linked to the EP type of ENSO; without SST variability in the WNP, ENSO is dominated by the central Pacific type. The WNP is thus an important contributor to ENSO diversity. The mechanism by which the WNP causes variations in the ENSO flavor is presented schematically in Fig. 9. The response of the ocean to the wind perturbations and ocean–atmosphere interactions that results in ENSO is determined by the initial state of the ocean. The presence of a charged oceanic heat content in the western equatorial Pacific (1) can lead to an anomalous deep atmospheric convection (2) at the surface that is characterized by strong surface divergence and diabatic cooling over the WNP and the Indian Ocean (3). Two off-equatorial Rossby waves (4) develop in response to this interaction with a band of westerlies sandwiched between them (5). The ocean responds to the westerlies by triggering equatorial Kelvin waves (6). Consequently, an El Niño can develop through the upwelling (7) of positive subsurface temperature anomalies (1) in the eastern tropical Pacific along the mean thermocline (8) by the eastward propagating Kelvin waves.

The WNP modulation stems from how it projects onto wind stress variations (4) in the western equatorial Pacific. When SST in the WNP is suppressed, wind stress anomalies in the western equatorial Pacific are equally muted. This leads to a weak recharge of the western Pacific warm water volume (1) and a shallow equatorial thermocline prior to the onset of an El Niño, which effectively weakens the ensuing Gill response (5–6) through a positive feedback loop. A weak Gill response begets weak and less frequent Kelvin waves that are characteristically unable to advect the warm subsurface ocean temperatures in the western equatorial Pacific all the way to the east. The upshot is the development of a central Pacific pattern of warming.

Our results are consistent with the general view that EP El Niño’s occur through oceanic Kelvin wave variability and feedbacks that engage the thermocline in the eastern Pacific, while CP events lack the classical thermocline feedbacks in the eastern Pacific and are more dependent on zonal advection feedbacks (Kug et al. 2009, 2010; Dommenges 2010; Ren and Jin 2013; Capotondi 2013). These varied mechanism are tied to the initial subsurface conditions in the

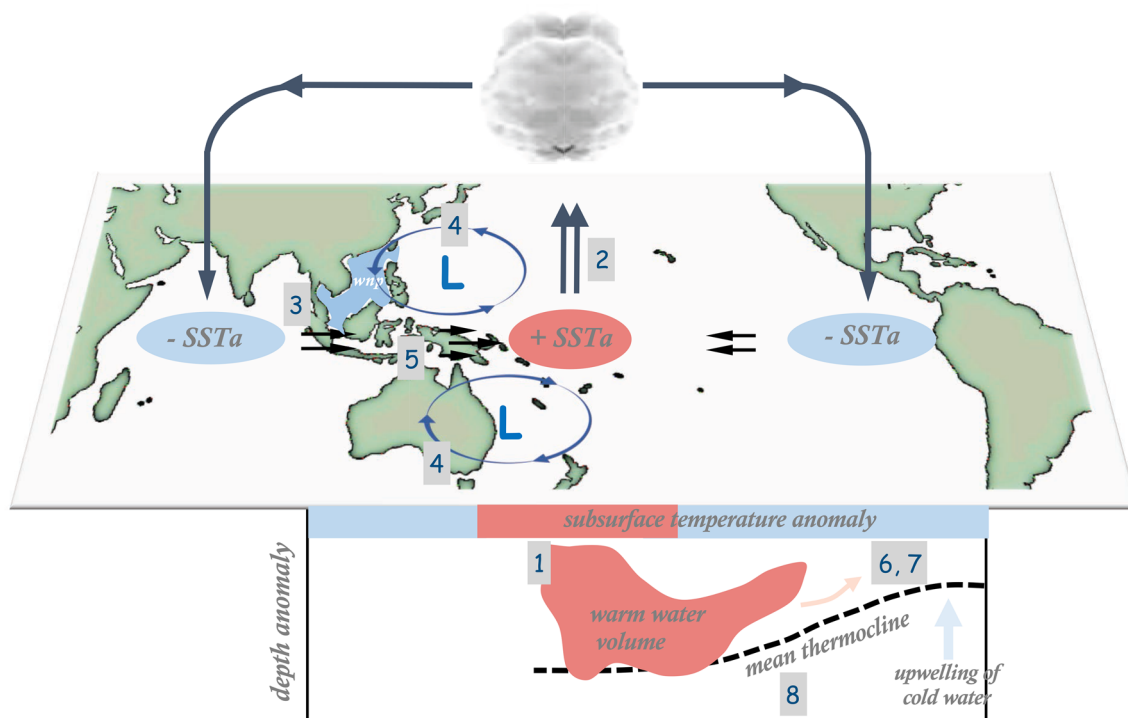


**Fig. 9** Schematic of the proposed mechanism for the impact of WNP on El Niño development

western equatorial Pacific—a deep (shallow) thermocline is said to favor the development of EP (CP) ENSO because of the relative dominance of thermocline (zonal advective) feedbacks under such a mean state (Fedorov et al. 2015; Capotondi and Sardeshmukh 2015; Xie and Jin 2018).

This study could also be relevant to the ongoing debate about whether indeed ENSO exists as two distinct modes of variability, or whether ENSO can be more aptly described as a diverse continuum (Capotondi et al. 2015). Our results seem to support the idea that ENSO is a continuum, and that a single physical ENSO mode could generate diversity in amplitude, spatial structure and temporal evolution (Giese and Ray 2011; Timmermann et al. 2018). CP ENSO events can thus be viewed as a variation of the EP type when the western equatorial Pacific is characterized by a shallow thermocline and weak westerly winds in the lead up to an El Niño event.

We expect that the results we have presented herein will contribute to our understanding of WNP–ENSO interactions. In particular, these results highlight the importance of WNP driven thermocline adjustments in causing ENSO diversity and advance our general understating of ENSO complexity. It also brings us a step closer to utilizing the WNP as a supplementary tool for useful seasonal ENSO predictions. Notwithstanding, we caution that our results may be model-dependent. Future work will include the determination of the extent to which such dependencies

are likely to affect the interpretation of our results. The modulation of the WNP precursor pattern by tropical intra-seasonal variability such as the MJO and other modes of climate variability on different timescales also warrant investigating.

**Acknowledgements** BF and JH thank Giovanni Liguori for his invaluable support with the CESM model and discussion on the SST-restoring impact on ENSO. BF thanks Yoshi Yoshimitsu Chikamoto for sharing his thoughts on ENSO complexity. SYS Wang is supported by U.S. Department of Energy under Award Number DE-SC0016605 and SERDP Award RC19-F1-1389. Computing and data storage resources, including the Cheyenne supercomputer (<https://doi.org/10.5065/D6RX99HX>), were provided by the Computational and Information Systems Laboratory (CISL) at NCAR. NCAR is sponsored by the National Science Foundation. This research was also supported in part through research cyberinfrastructure resources and services provided by the Partnership for an Advanced Computing Environment (PACE) at the Georgia Institute of Technology, Atlanta, Georgia, USA.

**Open Access** This article is licensed under a Creative Commons Attribution 4.0 International License, which permits use, sharing, adaptation, distribution and reproduction in any medium or format, as long as you give appropriate credit to the original author(s) and the source, provide a link to the Creative Commons licence, and indicate if changes were made. The images or other third party material in this article are included in the article's Creative Commons licence, unless indicated otherwise in a credit line to the material. If material is not included in the article's Creative Commons licence and your intended use is not permitted by statutory regulation or exceeds the permitted use, you will need to obtain permission directly from the copyright holder. To view a copy of this licence, visit <http://creativecommons.org/licenses/by/4.0/>.

## References

- Alexander MA, Vimont DJ, Chang P, Scott JD (2010) The impact of extratropical atmospheric variability on ENSO: testing the seasonal footprinting mechanism using coupled model experiments. *J Clim* 23(11):2885–2901
- Annamalai H, Xie SP, McCreary JP, Murtugudde R (2005) Impact of Indian Ocean sea surface temperature on developing El Niño. *J Clim* 18(2):302–319
- Anderson BT (2003) Tropical Pacific sea surface temperatures and preceding sea level pressure anomalies in the subtropical North Pacific. *J Geophys Res* 108(D23):4732
- Ashok K, Behera S, Rao AS, Weng H, Yamagata T (2007) El Niño Modoki and its teleconnection. *J Geophys Res* 112:11007
- Battisti DS, Hirst AC (1989) Interannual variability in a tropical atmosphere ocean model—influence of the basic state, ocean geometry and nonlinearity. *J Atmos Sci* 46:1687–1712
- Behringer DW, Xue Y (2004) Evaluation of the global ocean data assimilation system at NCEP: the Pacific Ocean, eighth symposium on integrated observing and assimilation system for atmosphere, ocean, and land surface. In: AMS 84th annual meeting, Seattle, Washington, pp 11–15
- Bjerknes J (1969) Atmospheric teleconnections from the equatorial Pacific. *Mon Weather Rev* 97:163–172
- Capotondi A (2013) ENSO diversity in the NCAR CCSM4 climate model. *J Geophys Res Oceans* 118:4755–4770
- Capotondi A, Sardeshmukh PD (2015) Optimal precursors of different types of ENSO events. *Geophys Res Lett* 42:9952–9960
- Capotondi A, Wittenberg AT, Masina S (2006) Spatial and temporal structure of tropical Pacific interannual variability in 20th century climate simulations. *Ocean Modell* 15:274–298
- Capotondi A, Wittenberg AT, Newman M, Lorenzo ED, Yu JY, Brannon P, Cole P, Dewitte B, Giese B, Guilyardi E, Jin FF, Karnauskas K, Kirtman B, Lee T, Schneider N, Xue Y, Yeh S (2015) Understanding ENSO diversity. *Bull Am Met Soc* 96(6):921–938
- Chang P, Zhang L, Saravanan R, Vimont DJ, Chiang JCH, Ji L, Seidel H, Tippett MK (2007) Pacific meridional mode and El Niño—Southern oscillation. *Geophys Res Lett* 34:L16608
- Chen HC, Sui CH, Tseng YH, Huang B (2015) An analysis of the linkage of Pacific subtropical cells with the recharge-discharge processes in ENSO evolution. *J Clim* 28(9):3786–3805
- Chiang JCH, Vimont DJ (2004) Analogous Pacific and Atlantic meridional modes of tropical atmosphere–ocean variability. *J Clim* 17:4143–4158
- Deser C, Phillips AS, Tomas RA et al (2012) ENSO and Pacific decadal variability in the community climate system model version 4. *J Clim* 25:2622–2651
- Di Lorenzo E, Liguori G, Schneider N, Furtado JC, Anderson BT, Alexander MA (2015) ENSO and meridional modes: a null hypothesis for Pacific climate variability. *Geophys Res Lett* 42(21):9440–9448
- Ding R, Li J, Tseng Y-H, Sun C, Guo Y (2015) The Victoria mode in the North Pacific linking extratropical sea level pressure variations to ENSO. *J Geophys Res Atmos* 120:27–45
- Dommenget D (2010) The slab ocean El Niño. *Geophys Res Lett* 37:L20701
- Fedorov AV, Hu SN, Lengaigne M, Guilyardi E (2015) The impact of westerly wind bursts and ocean initial state on the development, and diversity of El Niño events. *Clim Dyn* 44:1381–1401
- Gent PR et al (2011) The community climate system model version 4. *J Clim* 24:4973–5499
- Giese BS, Ray S (2011) El Niño variability in simple ocean data assimilation (SODA), 1871–2008. *J Geophys Res Oceans* 116:C02024
- Gill AE (1980) Some simple solutions for heat-induced tropical circulation. *Q J R Met Soc* 106:447–462
- Hu ZZ, Kumar A, Huang B, Zhu J, Zhang RH, Jin FF (2017) Asymmetric evolution of El Niño and La Niña: the recharge/discharge processes and role of the off-equatorial sea surface anomaly. *Clim Dyn* 49:2737–2748
- Izumo T, Vialard J, Lengaigne M, de Boyer MC, Behera SK, Luo J-J, Cravatte S, Masson S, Yamagata T (2010) Influence of the state of the Indian Ocean dipole on the following year's El Niño. *Nat Geosci* 3(3):168–172
- Jin FF (1997) An equatorial ocean recharge paradigm for ENSO. Part II: A stripped down coupled model. *J Atmos Sci* 54:830–847
- Kalnay E, Kanamitsu M, Kistler R, Collins W, Deaven D, Gandin L, Iredell M, Saha S, White G, Woollen J, Zhu Y, Chelliah M, Ebisuzaki W, Higgins W, Janowiak J, Mo K, Ropelewski C, Leetmaa A, Reynolds R, Jenne R (1996) The NCEP/NCAR 40-year reanalysis project. *Bull Am Meteor Soc* 77:437–471
- Kao H-Y, Yu J-Y (2009) Contrasting eastern-Pacific and central-Pacific types of El Niño. *J Clim* 22:615–632
- Karnauskas KB (2013) Can we distinguish canonical El Niño from Modoki? *Geophys Res Lett* 40:5246–5251
- Kim ST, Yu J-Y, Kumar A, Wang H (2012) Examination of the two types of ENSO in the NCEP CFS model and its extratropical associations. *Mon Weather Rev* 140:1908–1923
- Kirtman B (2019) Special issue: ENSO diversity. *Clim Dyn* 52:7133
- Kug J-S, Jin F-F, An S-I (2009) Two types of El Niño events: cold tongue El Niño and warm pool El Niño. *J Clim* 22:1499–1515
- Kug J-S, Choi J, An SI, Jin F-F, Wittenberg AT (2010) Warm pool and cold tongue El Niño events as simulated by the GFDL CM2.1 coupled GCM. *J Clim* 23:1226–1239
- Larkin NK, Harrison DE (2005) On the definition of El Niño and associated seasonal average U.S. weather anomalies. *Geophys Res Lett* 32:L13705
- Liguori G, Di Lorenzo E (2019) Separating the north and south Pacific meridional modes contributions to ENSO and tropical decadal variability. *Geophys Res Lett* 46:906–915
- McPhaden MJ (2004) Evolution of the 2002/03 El Niño. *Bull Am Meteorol Soc* 85(5):677–695
- Meinen CS, McPhaden MJ (2000) Observations of warm water volume changes in the equatorial Pacific and their relationship to El Niño and La Niña. *J Clim* 13:3551–3559
- Park JH, An SI, Kug JS (2017) Interannual variability of western North Pacific SST anomalies and its impact on North Pacific and North America. *Clim Dyn* 49:3787–3798
- Pegion K, Selman C (2017) Extratropical precursors of the El Niño–Southern oscillation. *Climate extremes: patterns and mechanisms*. Geophysical monograph series, vol 226. American Geophysical Union, Washington, DC, pp 299–314
- Rayner NA, Parker DE, Horton EB, Folland CK, Alexander LV, Rowell DP, Kent EC, Kaplan A (2003) Global analyses of sea surface temperature, sea ice, and night marine air temperature since the late nineteenth century. *J Geophys Res Atmos* 108(D14):4407
- Ren H-L, Jin F-F (2013) Recharge oscillator mechanisms in two types of ENSO. *J Clim* 26:6506–6523
- Rogers JC (1981) The north Pacific oscillation. *J Climatol* 1:39–57
- Schopf PS, Suarez MJ (1988) Vacillations in a coupled ocean-atmosphere model. *J Atmos Sci* 45:549–566
- Schott FA, Xie SP, McCreary JPJ (2009) Indian Ocean circulation and climate variability. *Rev Geophys* 47:RG1002
- Stuecker MF (2018) Revisiting the Pacific meridional mode. *Sci Rep* 8(1):1–9
- Takahashi K, Montecinos A, Goubanova K, Dewitte B (2011) ENSO regimes: reinterpreting the canonical and Modoki El Niño. *Geophys Res Lett* 38:L10704
- Taschetto AS, Gupta AS, Jourdain NC, Santoso A, Ummenhofer CC, England MH (2014) Cold tongue and warm pool ENSO events in CMIP5: mean state and future projections. *J Clim* 27:2861–2885

- Timmermann A, An S-I, Kug J-S, Jin F-F, Cai W, Capotondi A, Cobb K, Lengaigne M, McPhaden MJ, Stuecker MF, Stein K, Wittenberg AT, Yun K-S, Bayr T, Chen H-C, Chikamoto Y, Dewitte B, Dommenger D, Grothe P, Guilyard E, Ham Y-G, Hayashi M, Ineson S, Kang D, Kim S, Kim W, Santoso A, Takahashi K, Todd A, Wang G, Wang G, Xie R, Yang W-H, Yeh S-W, Hoon J, Zeller E, Zhang X (2018) El Niño-Southern Oscillation complexity. *Nature* 559:535–545
- Vasquez KAM (2015) The intraseasonal equatorial oceanic Kelvin wave and the central Pacific El Niño phenomenon. *Climatology*. Université Paul Sabatier - Toulouse III, 2015. English. NNT: 2015TOU30324
- Vimont DJ, Wallace JM, Battisti DS (2003) The seasonal footprinting mechanism in the Pacific: implications for ENSO. *J Clim* 16:2668–2675
- Vimont DJ, Alexander MA, Newman M (2014) Optimal growth of central and east Pacific ENSO events. *Geophys Res Lett* 41:4027–4034
- Wang SY, L'Heureux M, Chia HH (2012) ENSO prediction one year in advance using western north Pacific sea surface temperatures. *Geophys Res Lett* 39:2–7
- Wang S-Y, L'Heureux M, Yoon J-H (2013) Are greenhouse gases changing ENSO precursors in the western North Pacific. *J Clim* 26:6409–6322
- Wang SY, Jiang X, Fosu B (2015) Global eastward propagation signals associated with the 4–5-year ENSO cycle. *Clim Dyn* 44(9):2825–2837
- Xie R, Jin F-F (2018) Two leading ENSO modes and El Niño types in the Zebiak-Cane model. *J Clim* 31:1943–1962
- Xie SP, Philander SGH (1994) A coupled ocean-atmosphere model of relevance to the ITCZ in the eastern Pacific. *Tellus A* 46(4):340–350
- Yoon J-H, Wang SYS, Gillies RR, Kravitz B, Hipps L, Rasch PJ (2015) Increasing water cycle extremes in California and in relation to ENSO cycle under global warming. *Nat Commun* 6:8657
- You YJ, Furtado JC (2017) The role of south Pacific atmospheric variability in the development of different types of ENSO. *Geophys Res Lett* 44(14):7438–7446
- Yu J-Y, Fang S-W (2018) The distinct contributions of the seasonal footprinting and charged-discharged mechanisms to ENSO complexity. *Geophys Res Lett* 45:6611–6618
- Yu J-Y, Kim ST (2011) Relationships between extratropical sea level pressure variations and the central Pacific and eastern Pacific types of ENSO. *J Clim* 24:708–720
- Yu LS, Rienecker MM (1999) Mechanisms for the Indian Ocean warming during the 1997–98 El Niño. *Geophys Res Lett* 26:735–738
- Zhang H, Clement A, Di Nezio P (2014) The south Pacific meridional mode: a mechanism for ENSO-like variability. *J Clim* 27:769–783

**Publisher's Note** Springer Nature remains neutral with regard to jurisdictional claims in published maps and institutional affiliations.